X-ray and Magnetic Characterization of a Nematic Polyester Based on a Metallomesogenic Copper(II) Moiety

P. J. Alonso,† J. A. Puértolas,† P. Davidson,‡ B. Martínez,§ J. I. Martínez,† L. Oriol,† and J. L. Serrano*,†

Instituto de Ciencia de Materiales de Aragon, Universidad de Zaragoza, Consejo Superior de Investigaciones Científicas, Plaza S. Francisco s/n, 50009 Zaragoza, Spain, Laboratoire de Physique des Solides, Université Paris-Sud, Bâtiment 510, Centre Universitaire, 91405 Orsay Cedex, France, and Institut de Ciencia de Materials, Consejo Superior de Investigaciones Científicas, Campus de la UAB, 08193 Bellaterra, Spain

Received October 28, 1992; Revised Manuscript Received April 13, 1993

ABSTRACT: A structural and magnetic study of a copper-containing nematic polyester has been carried out. X-ray diffraction, magnetization, and EPR experiments on samples with different thermal histories have been performed. In powdered samples, changes in magnetic properties are related to thermally induced structural modifications. A detailed study of a nematic melt-drawn fiber was made. The fiber displayed a large nematic order parameter and a parallel alignment of the copper coordination planes with the stretching direction.

1. Introduction

In recent years, the synthesis of polymers which incorporate metals in their structure has been of increasing interest, especially side and main chain metal-containing liquid crystal polymers (LCP).[1] The possibility of introducing metal atoms at specific points of a molecule which can easily be oriented in the mesophase endows these materials with potentially interesting properties. Recent advances have been reported with low molecular weight metallomesogens.[2] Polymeric materials with similar properties have a higher processability. In this way macroscopically oriented fibers or films can be obtained.[3]

In the field of metallomesogens we have paid special attention to the synthesis of paramagnetic materials of both high and low molecular weight.[4] The interaction of a magnetic field with these materials leads to macroscopic orientation of the molecules. Depending on the structure of the molecules this orientation is either parallel or perpendicular to the magnetic field.[5] With regard to metals, derivatives of Cu(II) have been shown to be of great interest because of their thermal stability and the high paramagnetic contribution of the metal to the anisotropy of the magnetic susceptibility.[6] This contribution has a great influence on the molecular orientation in the presence of a magnetic field.

In a previous paper[7] we described a family of metallomesogen main chain polyesters derived from Cu(II) complexes. These materials combine the formerly-mentioned properties and are representative examples of paramagnetic LCP. Here we report the structural and magnetic properties of a representative member, coded as [N7Cu][P10]. The polymer was obtained by interfacial polycondensation and was chosen because of its relatively low transition temperatures and the range of enantiotropic nematic mesophase.

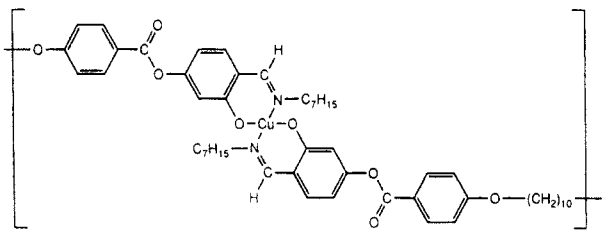

[N7Cu][P10]

To study magnetic properties in relation to thermally-induced structural changes, different samples were prepared:

Sample I is the polymer as obtained. It is a semicrystalline material showing a nematic phase.

Sample II is an annealed sample. Sample I was annealed close to T_m to increase its crystallinity.

Sample III was obtained by quenching from the nematic melt to obtain a frozen nematic phase.

Fibers: A structural study based on X-ray diffraction and EPR measurements was carried out with fibrous samples obtained from the nematic state.

2. Experimental Section

Materials. The polymer was synthesized using the interfacial polycondensation method: 2 mmol of sodium hydroxide and 1 mmol of bis(*N*-heptyl-4-hydroxysalicylaldiminate)copper(II) were dissolved in 25 mL of a water–dioxane mixture (4:1). Aliquat 336 (355 mg) as a phase transfer catalyst in 1 mL of dioxane was added, and the mixture was stirred slowly. A solution of 1 mmol of 1,10-bis[(chloroformyl)phenoxy]decane in 10 mL of chloroform was added quickly, and the mixture was stirred at 3600 rpm for 30 min. The polymer was obtained by pouring the resulting mixture into 150 mL of methanol, filtering, and washing with water, methanol, and acetone. The polymer was dried under vacuum over P_2O_5 at 80 °C for 24 h. Elemental analysis (calculated in parentheses): % C, 70.15 (68.59); % H, 7.95 (7.31); % N, 2.65 (3.08). The polymer showed an inherent viscosity η_{inh} of 0.16 dL/g, which was determined using a Cannon-Fenske viscosimeter at a concentration of 0.5 g/dL in 1,1,2,2-tetrachloroethane at 50 °C. Samples of polymer as obtained (untreated) were coded as sample I. From this starting material, three different samples were prepared: sample II was obtained by

* To whom correspondence should be addressed.
† Instituto de Ciencia de Materiales de Aragon.
‡ Université Paris-Sud.
§ Institut de Ciencia de Materials.

0024-9297/93/2226-4304$04.00/0

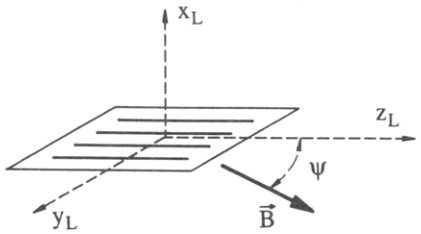

Figure 1. Experimental arrangement for EPR measurements of fiber samples. Ψ gives the magnetic field orientation relative to the fiber axis.

annealing at 150 °C for 1 h; sample III was prepared by quenching the sample from the nematic state (195 °C, 10 min) into liquid nitrogen to obtain nematic glasses; fibers were drawn from the nematic phase at approximately 195 °C into air at room temperature with preheated tweezers (very large fibers can easily be obtained using this procedure).

Techniques. DSC measurements were conducted with a Perkin-Elmer DSC-7 apparatus calibrated with indium (mp 156.6 °C, heat of fusion 28.4 J/g) and tin (mp 321.9 °C, heat of fusion 60.4 J/g) using powdered samples (about 7 mg) in aluminum pans. The scan rate was 10 °C/min. Transition temperatures were read at the maximum of the peak.

Mesogenic behavior was checked in a Nikon polarizing microscope fitted with a Mettler FP-82 heating stage and an FP-80 control unit.

X-ray diffraction patterns were obtained with a simple X-ray setup. A point-focused monochromatic (λ(Cu Kα) = 1.541 Å) X-ray beam was obtained by reflection on a doubly-bent pyrolitic graphite slab. The samples were mounted in an air-evacuated commercial camera (Unicam). The diffracted X-rays were collected on a flat film at a distance of 80 mm from the sample.

EPR measurements were taken with a Varian E-112 spectrometer working in the X-band. The powdered samples were measured by introducing them into a standard EPR quartz tube (707-SQ from Wilmad). Fibers obtained from the nematic phase were aligned by gluing them on Scotch tape and then mounting on a rotating setup attached to a goniometer. Magnetic field orientation dependence of the spectra will be referred to the Ψ angle as shown in Figure 1.

Magnetic measurements of the polysemicrystalline samples were performed on a SHE magnetometer, equipped with a SQUID sensor. Magnetization measurements, $M(H)$, at 2.5 and 5.0 K were carried out varying the magnetic field H from a few oersted to 50 kOe. Static magnetic susceptibility, $\chi(T)$, was obtained at 25 kOe and at different temperatures from room temperature to 5 K. The samples were packed in a gelatin capsule holder, and their weights were close to 0.035 g.

3. Results and Discussion

3.1. Thermal Characterization. The polymer is a member of a family of metallomesogenic polyesters whose thermal and mesogenic behavior has been extensively discussed elsewhere.[7] With respect to this polymer, it displays an enantiotropic nematic mesophase which was characterized by observation of the samples in the polarizing optical microscope at different temperatures. A threaded texture was easily observed and under mechanical stress a marbled texture appeared. Transition temperatures were determined by DSC. In the first heating run two endothermic contributions corresponding to melting (T_m = 188 °C) and isotropization (T_i = 213 °C) appeared. The second heating showed a cold crystallization and three endothermic peaks. The presence of an exothermic peak (cold crystallization at 113 °C) points to the possibility of obtaining nematic glasses at room temperature by cooling the nematic melt. Optical observations corroborate this hypothesis, and frozen nematic textures can be observed at room temperature. The three endothermic peaks of the second heating correspond to a crystal–crystal transition ($T_{K-K'}$ = 166 °C), melting (T_m = 186 °C), and isotropization (T_i = 205 °C).

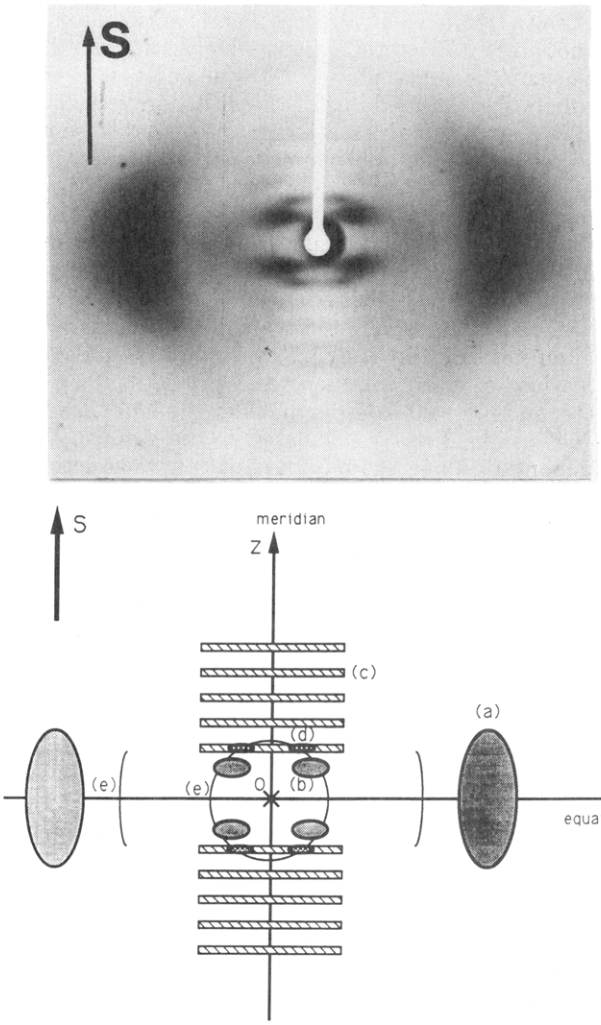

Figure 2. (a, Top) X-ray diffraction pattern of a frozen nematic fiber. S represents the stretching direction. (b, Bottom) Schematic representation of the pattern in (a). O is the origin of the reciprocal space which has a uniaxial symmetry around the meridian Oz (stretching direction). a, b, c, d, and e represent the different scattering elements as described in the text.

In sample II an increase of ca. 20% in enthalpy of the melting transition was observed in the melting with respect to the untreated polymer. The nematic glass (sample III) exhibits a T_g = 55 °C in DSC measurements.

3.2. X-ray Diffraction Experiments. At room temperature sample I exhibits a mixture of roughly 10% of crystalline phase and 90% of amorphous phase. The crystallinity ratio is therefore about 10%. Samples annealed at 150 °C for 1 h (sample II) reach a crystallinity ratio of about 50%. This behavior is typical of a semicrystalline polymer. The crystalline phase increases significantly during the annealing. DSC measurements are qualitatively in agreement with the X-ray data, and the DSC curve of sample II shows an increase in ΔH_m corresponding to the melting transition with respect to sample I. In the nematic quenched sample (sample III) the existence of ca. 5% of crystalline phase is detected. This can be attributed to partial crystallization during the quenching.

A single domain nematic ordering using magnetic fields was not obtained due to the high viscosity of the nematic phase and the high transition temperatures. Fibers were drawn from the nematic melt to obtain macroscopically oriented samples. The results of the X-ray diffraction of these fibers are interesting, and the following discussion is focused on these experiments.

Figure 2 shows the X-ray diffraction pattern of a nematic

melt-drawn fiber. This pattern is clearly anisotropic and does not present Bragg reflections, which is characteristic of an oriented nematic phase.[8] At wide angles ($s \approx 1/4.5$ Å^{-1}, where s is the modulus of the diffusion vector, $s = (2 \sin \theta)/\lambda$, and 2θ is the scattering angle), a diffuse ring (a) located in the equatorial plane shows that the mesogenic cores, which contain copper ions, are oriented along the stretching direction. The polar angular extension of this ring is rather small, indicating that the nematic order parameter S is large ($S \approx 0.8$) and that the polymer chains are on the whole well aligned.

At small angles, strong diffuse spots (b) outside the meridian indicate the presence of important smectic C fluctuations of correlation lengths $\xi_{b\parallel} \approx 50$ Å along the director and $\xi_{b\perp} \approx 30$ Å perpendicular to it. The tilt angle $\alpha_b \approx 55°$ can be directly calculated on the pattern. The component s_{zb} along the meridian of the wavevector s_b relative to these diffuse spots b takes the value $s_{zb} \approx 1/30$ Å^{-1}, whereas the molecular length of the repeating unit is $L = 36 \pm 1$ Å as measured on Dreiding stereomodels (for its most extended conformation). Therefore, the conformation of the repeating unit when submitted to these S_C fluctuations is very different from the fully extended one.

When closely inspected, this X-ray diffraction pattern also displays a set of equidistant straight lines (c) which represent the intersection with the Ewald sphere of a set of planes perpendicular to the meridian and equidistant with a period $s_{zc} \approx 1/35$ Å^{-1}. This set of diffuse planes is due to the existence in the nematic phase of short-range linear correlations between the mesogenic cores,[9,10] namely, the presence of completely uncorrelated rows of equally spaced moieties. Here, the origin of these rows is obviously due to the nature of the main chain polymer. In fact, the row periodicity is about equal to that of the repeating unit, and the correlation length $\xi_{c\parallel} \approx 200$ Å of this linear short-range order represents a calculation of some kind of polymer persistence length. This length roughly corresponds to ten polymer repeating units.

The intensity of the second diffuse line is clearly modulated, resulting in the appearance of the weak and small diffuse spots d. The third diffuse line is also slightly modulated, whereas this modulation cannot be properly observed in the first diffuse line because of the presence of the diffuse spots b. These diffuse line intensity modulations can be explained by the existence of another kind of S_C fluctuation. The diffuse spots (d) are weaker and smaller than the b ones, which means that the second kind of S_C fluctuations are of smaller size but somewhat larger correlation lengths ($\xi_{d\parallel} \approx 200$ Å, $\xi_{d\perp} \approx 50$ Å) than those of the first kind. The tilt angle is $\alpha_d \approx 25°$ and the component s_{zc} of the wavevector s_d relative to these diffuse spots d is $s_{zd} = 2/35$ Å^{-1}. The two kinds of S_C fluctuations coexist independently in the nematic phase.

Taking into account these different short-range orders b, c, and d, the molecular organization of the polymer in its nematic phase can be summarized considering that the polymer displays, essentially, two kinds of conformation. The first one of length $L_b \approx 30$ Å gives rise to the S_C fluctuations responsible for the diffuse spots b. The second conformation of length $L_c \approx 35$ Å $\approx L$ is present in the completely extended polymer sections which give rise to the diffuse scattering c. These same sections also present the second type of S_C fluctuations and then give rise to the diffuse scattering d. Similar behavior was observed in phasmidic molecules[10] which in the nematic phase present two kinds of conformation. One of these conformations has a length equal to that of the completely extended molecule and gives rise to linear correlations whereas the other conformation has a markedly shorter length and gives rise to a strong S_C short-range order.

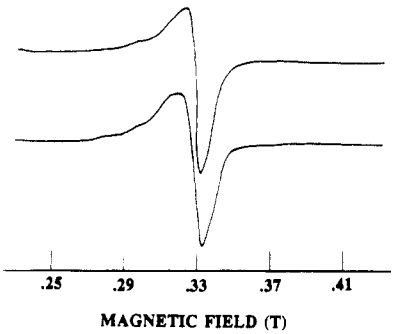

Figure 3. Room temperature EPR spectra of sample I or II (upper trace) and of sample III (lower trace).

The determination of the first conformation of the repeating unit which gives rise to the diffuse scattering b as well as the determination of the relative proportions of both conformations cannot be derived from these X-ray scattering experiments and must be obtained by other techniques. Moreover, no diffuse scattering could be detected in Figure 2 which would have indicated some Cu–Cu correlations between neighboring mesogenic cores. Such Cu–Cu correlations (around $s = 1/8.5$ Å^{-1}) were previously reported in the S_A phase of a mesogenic Cu complex involving two Schiff bases and interpreted by pairing of the complexes.[11] This effect was not observed in the nematic phase of our polymer; this was also the case with several Cu complexes in the same homologous series as the polymer repeating unit.[12]

The above-described molecular organization of the nematic phase studied on a highly stretched sample may be different from that of the thermodynamic equilibrium state. To check this point, several attempts were made to align the nematic phase in a magnetic field of 1.7 T. These attempts failed as the samples decomposed during the annealing for several hours at about 200 °C. However, powder X-ray diffraction patterns of bulk quenched samples from the nematic state (sample III) confirm the nematic nature of the mesophase and displayed a small-angle diffuse ring due to the S_C fluctuations. However, such powder patterns did not allow us to check whether the second type of S_C fluctuations were also present in the bulk samples since the diffuse spots d become a diffuse ring hidden by the diffuse spots b.

When carefully examined, the X-ray diffraction pattern presented in Figure 2 also reveals some extremely faint but very sharp diffraction lines (e) which are due to a small amount (<1%) of crystalline phase. This shows that the fiber-obtaining process was not fast enough to prevent crystallization completely. The first diffraction line goes through diffuse spot d though this spot is weaker than b. This can be understood by taking into account that the crystallization of well-extended polymer sections is easier. The crystalline phase itself is not readily obtained free of the nematic phase. It is noteworthy that the fibers remain unchanged at room temperature for up to 3 months. No recrystallization was observed after this time, and the X-ray diffractograms were reproducible.

3.3. EPR Measurements. The EPR spectra of sample I (as prepared) and sample II (annealed at 150 °C for 1 h) were measured at room temperature. No differences were found between the spectra of both types of sample. The top trace of Figure 3 displays the spectrum of these samples. The EPR spectrum at room temperature of sample III can be seen in the lower trace of Figure 3. No modification of these spectra was found when they were measured at liquid nitrogen temperature. Both are very similar and they show a *perpendicular* feature in their high-field region ($g \approx 2.06$) which shows no resolved

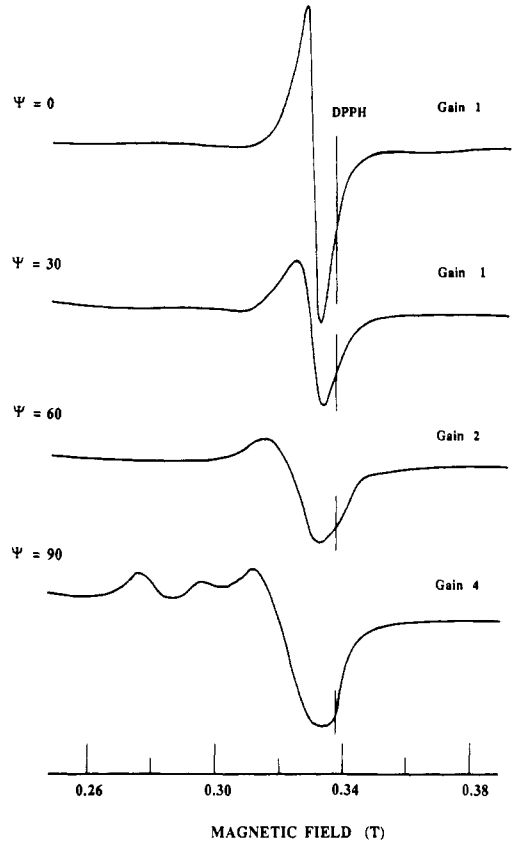

Figure 4. Room temperature EPR spectra of a fiber sample measured with different magnetic field orientation.

hyperfine structure and *parallel* features that can be associated with the hyperfine components of the *parallel* Cu(II) signal. The only difference between the spectra of semicrystalline samples (samples I and II, Figure 3 (top)) and the nematic glass (sample III, Figure 3 (bottom)) is the width of the lines, which proved to be broader in the former (half-width of the absorption shape greater than 7 mT) than in the quenched nematic sample (half-width of the absorption shape less than 6 mT).

EPR spectra of fiber samples were also measured. In these cases the EPR signal is anisotropic and it depends on the magnetic field orientation (given by Ψ; see Figure 1). In Figure 4 we show this spectrum for different values of Ψ. When the magnetic field is oriented along the fiber axis, only the *perpendicular* signal (high-field side) is observed. As the magnetic field is rotated, the spectrum extends toward the low-field region in such a way that when the magnetic field is perpendicular to the fiber (Ψ = 90) the spectrum shows the *parallel* and the *perpendicular* features, the former contribution being higher in this case than the perpendicular one as compared with the spectra of semicrystalline samples (see Figure 3 (top)). Also noteworthy is the difference in the width of the perpendicular contribution, which increases as the angle Ψ does.

The same spin Hamiltonian can be used to explain all the experimental results:

$$\mathcal{H} = \mu_B\{g_\perp(S_xB_x + S_yB_y) + g_\parallel S_zB_z\} + A_\perp(S_xI_x + S_yI_y) + A_\parallel S_zI_z \quad (1)$$

with $g_\parallel = 2.23$, $g_\perp = 2.05$, $A_\parallel = 520$ MHz, and $A_\perp < 30$ MHz. These values are typical for divalent copper in a square-planar environment with its unpaired electron in a $|x^2 - y^2\rangle$ orbital.

The spectra of the polydomain or polysemicrystalline samples are immediately understood in the light of this. Computer simulations of the spectra were performed using

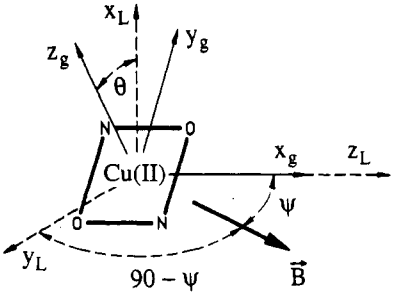

Figure 5. Sketch of the environment of Cu(II) and its orientation in a fiber sample. Ψ gives the magnetic field orientation, and θ values are randomly distributed in the [0,2π] range.

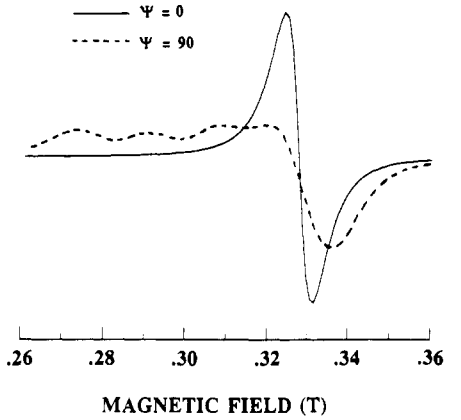

Figure 6. Calculated spectra of a fiber with the magnetic field parallel (—) and perpendicular (- - -) to the fiber axis. For details of the calculation, see text.

either Lorenztian or Gaussian line shapes. Good fits are obtained in both cases, indicating that the actual line shapes are neither Gaussian nor Lorentzian but somewhere between the two. Since the hyperfine structure remains resolved, at least in the *parallel* trace, and has values which are typical of isolated Cu^{2+}, the influence of the exchange in the EPR spectrum of the different polymer samples can be ruled out. Therefore the differences in the broadening of the lines between sample III and semicrystalline samples (samples I and II) are related to the dipolar broadening of the lines. Since the second moment of the transition is proportional to $\mathbf{r}^{-6}$, $\mathbf{r}$ being a typical intermolecular distance,[13] the former differences in the half-width of the transitions are understood when it is taken into account that the Cu^{2+}–Cu^{2+} distances are greater in the nematic phase than in the semicrystalline phase as a result of the translational freedom degree. On the other hand, the probable greater ordering of the annealed sample (sample II) as compared with the untreated sample (sample I) has no influence on this dipolar broadening.

The fiber spectra can be also understood if the fiber axis lies in the plane of the four nearest neighbors of copper while the normal to this square is randomly oriented in the plane normal to the fiber, so, with regard to Figure 5 the orientation of the magnetic field gives Ψ whereas θ takes any value between 0 and 180° at random. This arrangement agrees with the X-ray diffraction studies. Computer simulation of the fiber spectra as a function of the angle Ψ have been performed, assuming either a Lorentzian or a Gaussian line shape. In Figure 6 we show the calculated spectra using a Lorentzian line shape in the case of Ψ = 0° and Ψ = 90° (magnetic field parallel and perpendicular to the fiber axis) where the relative intensities of both traces have been fitted to those of the corresponding experimental spectra shown in Figure 4. There is a good agreement between the experimental results and the calculated spectra but some discrepancies arise mainly in the calculated spectrum for Ψ = 90°. This is due to the fact that the relative orientations of the

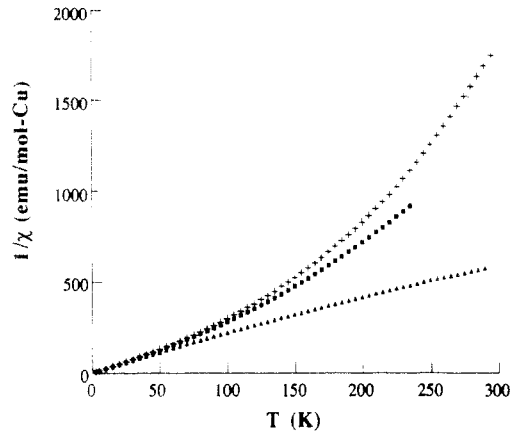

Figure 7. Reciprocal of the magnetic susceptibility as a function of the temperature $\chi^{-1}(T)$ for the three types of samples: (+) untreated; (▲) annealed; and (■) nematic glass.

Table I. Magnetic Parameters Obtained by Fitting Equation 2 to Data of Figure 8 (See Text)

	sample		
	untreated	annealed	frozen nematic
C (emu K/mol)	0.430	0.426	0.442
Θ (K)	−0.28	−0.25	−0.34
χ_0 (emu/mol)	-9.4×10^{-4}	$+2.6 \times 10^{-4}$	-8.3×10^{-4}

moieties in the nematic fibers are not completely parallel as follows from the diffraction data ($S \approx 0.8$), and also, as previously mentioned, the actual line shape is neither a true Lorentzian nor a true Gaussian curve. These two assumptions were taken into account in our calculation.

In spite of these discrepancies a strong magnetic field orientation dependence of the line width can be observed from our results. This anisotropy in the peak-to-peak width is due to an anisotropic dipole–dipole interaction. Taking into account that the shortest Cu–Cu distance along the polymer is about 35 Å while between adjacent chains it is in the 6–8-Å range, the main effect of the dipole–dipole contribution to width is due to the *lateral* interaction, which is responsible for this anisotropy in the line width. A rough calculation taking into account the above distance gives a ratio for the width of the lines for $\Psi = 90°$ and $\Psi = 0°$ ranging between 1.8 and 1.9. The curves in Figure 6 have been calculated with $\Delta B_{pp}(0) = 70$ G and $\Delta B_{pp}(90) = 130$ G and, consequently, with $\Delta B_{pp}(90)/\Delta B_{pp}(0) = 1.85$.

3.4. Magnetic Characterization. The temperature dependence of the reciprocal of the susceptibility, $1/\chi(T)$ is shown in Figure 7 for the three types of powdered samples (samples I, II, and III). At a high temperature the measurements show a strong deviation from the Curie–Weiss behavior, which could be due to the presence of an independent temperature susceptibility. So, we have fitted the data considering the superposition of a background susceptibility χ_0 and a Curie–Weiss contribution.

$$\chi_{exp} = \chi_0 + \frac{C}{T - \Theta} \qquad (2)$$

The values for the Curie constant (C), the Curie–Weiss temperature (Θ), and the χ_0 obtained from the fit at a suitably high temperature are presented in Table I. The results of these fits are shown in Figure 8.

The effective magnetic moments for Cu(II) in these samples determined from the Curie constant C are between 1.85 and 1.88 μ_B. The corresponding g values calculated with an $S = {}^1/_2$ spin are in the range $g = 2.13$–2.17, about 2–3% larger than those obtained from EPR measurements on the same powdered samples, which is in agreement

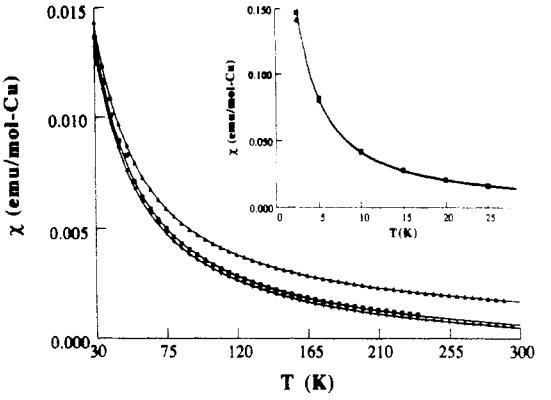

Figure 8. Thermal evolution of the susceptibility $\chi(T)$ of the three types of sample: (+) untreated; (▲) annealed, (■) nematic glass. Solid lines give the evolution of the susceptibility predicted using eq 2 with the data in Table I. A detail of the low-temperature evolution is shown in the inset.

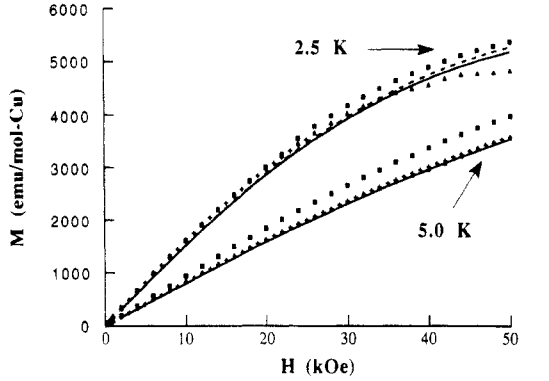

Figure 9. Magnetic field dependence of the magnetization measured at two different temperatures for the three types of samples: (+) untreated; (▲) annealed; (■) nematic glass. Lines gives the evolution predicted using eq 3 with the data in Table I: (—) untreated and annealed samples; (- - -) line for nematic glasses.

with the accuracy of the Cu mass analysis data of these samples.

A weak antiferromagnetic behavior with a Curie–Weiss temperature $\Theta = -0.3$ K appears in all the samples, indicating that the exchange interaction between Cu(II) is very small, according to the analysis of the EPR spectra. The resonance results indicate that the exchange interaction, if any, is weak enough to produce J/k_B values which are lower than 0.1 K.

The inset of Figure 8 plots the extrapolation at low temperatures of the former fit. A small deviation from the experimental data below 5 K is observed, in agreement with the Θ values obtained.

Finally and with regard to the background susceptibility χ_0, the results show diamagnetic behavior for nematic and virgin samples ($\chi_0 \approx -0.009$ emu/mol of Cu) and small paramagnetic behavior ($\chi_0 \approx +0.0003$ emu/mol of Cu) for the annealed samples.

Magnetization values as a function of the dc magnetic field, $M(H)$, measured at 2.5 and 5.0 K and corrected for the independent temperature term, $\chi_0 H$, are presented in Figure 9. We also show the results of the molecular field theory (MF) for $S = {}^1/_2$

$$M(H) = M_s \tanh\left\{\frac{gS\mu_B H}{k_B T} + \frac{\Theta M}{T M_s}\right\} \qquad (3)$$

calculated with the Θ and g values obtained from the high-temperature susceptibility analysis and M_s being the saturation magnetization ($M_s = NgS\mu_B$). For samples I and II, a good agreement is obtained at 5 K, and a small deviation is observed at 2.5 K, according to the Curie–

Weiss behavior. However, we cannot account for the departure of the nematic glass sample data, mainly at 5 K.

The former magnetic properties seem to indicate that the most noticeable difference between the different powdered samples corresponds to the background contribution χ_0 of the annealed sample as compared with that of the other two samples.

Since the untreated (I) and quenched nematic (III) samples have an amorphous character with a positional disorder in the magnetic sites and since the distance between them is sufficiently great, we could consider the exchange interaction negligible and therefore obtain paramagnetic behavior. The order introduced in the S_C fluctuating regions does not affect this behavior. For the annealed sample, the higher enthalpy content in the melting transition and the microstructure obtained by X-rays show a higher degree of crystallinity. The crystal region does not seem to cause great variations in the Cu(II) distances according to EPR data, and consequently the annealed sample is also in the paramagnetic state. However, the high polymerization seems to induce changes in the background susceptibility, χ_0.

To carry out a qualitative analysis of χ_0, we considered the presence of two terms, one of them a diamagnetic contribution related to the organic molecule and the other, a temperature-independent paramagnetism (TIP) associated with Cu(II). The latter arises from a mixing in the ground state of the excited states which are not thermally populated. Evidence of this behavior for Cu(II) is observed, for instance, in heteropoly complexes[14] in which Cu(II) has an octahedral coordination with oxygen atoms in the vertex. In these compounds the paramagnetic sites are embedded in a giant diamagnetic molecule. The TIP contribution obtained for two different compounds of that series were $\chi_0 = 2.0 \times 10^{-4}$ emu/mol of Cu and $\chi_0 = 37.5 \times 10^{-4}$ emu/mol of Cu.

In our case, the EPR measurements point to the same square-planar environment for the three samples. Therefore, the way to obtain an effective positive contribution in χ_0 is by means of a decrease in the diamagnetic term. This behavior was also found in magnetic studies of Cu-based organometallic polymers[15] in which the lower molecular weight polymer is diamagnetic and the high molecular weight is paramagnetic. The authors do not explain this phenomenon. We thought that only a reduction in the number of conformations which contribute to the diamagnetic term due to the limitation of mobility which produces the higher polymerization could decrease the diamagnetic contribution to χ_0 and evidence the TIP effect.

To evaluate quantitatively this phenomenon, a study of polymers of the same family with nonparamagnetic metallic atoms is not sufficient. Consequently, we measured the background χ_0, but when the TIP of the new atoms was known, we were able to separate the diamagnetic term and determine the influence of molecular weight on magnetic behavior.

4. Conclusions

Electron paramagnetic resonance (EPR), magnetization, and susceptibility measurements indicate that all the samples show paramagnetic behavior with a weak exchange interaction of antiferromagnetic character between copper ions. The different degrees of crystallinity detected by X-ray diffraction have no influence on the magnetic interactions. However, these degrees of crystallinity do influence the background susceptibility via diamagnetic contribution.

EPR measurements indicate that the environment of copper is square planar in all the samples. Analysis of the angular evolution of the EPR spectra in fibers of metalloorganic polymers provides structural information about the orientation of the metal in the polymer chain, indicating that the vector perpendicular to the copper coordination plane is randomly perpendicular to the fiber axis. This is in agreement with the X-ray diffraction observations which show that the mesogenic cores containing copper atoms are oriented along the stretching direction. Polymer chains are on the whole well aligned with a high order parameter ($S \approx 0.8$). This orientation remains unchanged after keeping the fiber at room temperature for over 3 months.

X-ray diffraction also shows that the polymer repeating unit can adopt essentially two kinds of conformations in the nematic phase. The first one of length $L_b \approx 30$ Å induces strong S_C fluctuations, whereas the second one of length $L_c \approx 35$ Å is the fully extended conformation which promotes linear correlations and eventually crystallization.

Acknowledgment. This work was partially supported by the CICYT (Spain) under Contracts MAT 90-0748 and MAT89-0531-CO2-02. The authors would like to thank Dr. A. M. Levelut for her helpful comments.

References and Notes

(1) (a) Takahashi, S.; Murata, E.; Kariya, M.; Sonogashira, K.; Hagihara, N. *Macromolecules* **1979**, *12*, 1016; (b) Carfagna, C.; Caruso, U.; Roviello, A.; Sirigu, A. *Makromol. Chem., Rapid Commun.* **1987**, *8*, 345; (c) Moore, J. S.; Stupp, S. I. *Polym. Bull.* **1988**, *19*, 251; (d) Hanabusa, K.; Higashi, J.; Koyama, T.; Shirai, H. *Makromol. Chem.* **1989**, *190*, 1; (e) Singh, P.; Rausch, M. D.; Lenz, R. W. *Polym. Bull.* **1989**, *22*, 247; (f) Wu, F.; Zhang, R.; Jiang, Y. *Chin. J. Polym. Sci.* **1991**, *9*, 71.

(2) (a) Piechocki, C.; Simon, J.; Skoulious, A.; Guillon, D.; Weber, P. *J. Am. Chem. Soc.* **1982**, *104*, 5254; (b) Haase, W.; Borchers, B. In *Magnetic Molecular Materials*; Gatteschi, D., Khan, O., Miller, J. S., Palacio, F., Eds.; NATO ASI Series (Series C); Kluwer Academic: The Netherlands, 1991; p 245; (c) Matsuzaki, H.; Yamamoto, I.; Kazuchita, O. Jpn. Kokai Tokkyo Koho, Appl. 86/73262, 1986.

(3) (a) Hanabusa, K.; Tanimura, Y.; Suzuki, T.; Koyama, T.; Shirai, H. *Makromol. Chem.* **1991**, *192*, 233; (b) Caruso, U.; Roviello, A.; Sirigu, A. *Macromolecules* **1991**, *24*, 2606.

(4) (a) Serrano, J. L.; Romero, P.; Marcos, M.; Alonso, P. J. *J. Chem. Soc., Chem. Commun.* **1990**, 860; (b) Marcos, M.; Romero, P.; Serrano, J. L. *Chem. Mater.* **1990**, *2*, 495; (c) Marcos, M.; Oriol, L.; Serrano, J. L.; Alonso, P. J.; Puértolas, J. A. *Macromolecules* **1990**, *23*, 5187.

(5) Marcos, M.; Serrano, J. L. *Adv. Mater.* **1991**, *30*, 256 and references therein.

(6) Barberá, J.; Levelut, A. M.; Marcos, M.; Romero, P.; Serrano, J. L. *Liq. Cryst.* **1991**, *10*, 119.

(7) Marcos, M.; Oriol, L.; Serrano, J. L. *Macromolecules* **1992**, *25*, 5362.

(8) See, for instance: Azaroff, L. V. *Mol. Cryst. Liq. Cryst.* **1987**, *145*, 31 and references therein.

(9) Doucet, J.; Lambert, M.; Levelut, A. M. *J. Phys. (Paris)* **1971**, *32*, C5a-247.

(10) Levelut, A. M.; Fang, Y.; Destrade, C. *Liq. Cryst.* **1989**, *4*, 441.

(11) Levelut, A. M.; Ghedini, M.; Bartolino, R.; Nicoletta, F. P.; Rustichelli, F. *J. Phys. (Paris)* **1989**, *50*, 113.

(12) Marcos, M.; Romero, P.; Serrano, J. L.; Barberá, J.; Levelut, A. M. *Liq. Cryst.* **1990**, *7*, 251.

(13) Slitcher, C. P. In *Principles of Magnetic Resonance*, 3rd ed.; Springer-Verlag: New York, 1990; Chapter 3.

(14) Gomez-García, C. J.; Casan-Pastor, N.; Coronado, E.; Baker, L. C. W.; Pourroy, G. *J. Appl. Phys.* **1990**, *67*, 5995.

(15) Zuo, F.; Yu, I.; Salamon, M. B.; Hong, X.; Stupp, S. I. *J. Appl. Phys.* **1991**, *69*, 7951.